Inorganic Chemistry

Article

pubs.acs.org/IC

Cu^{2+}, Zn^{2+}, and Ni^{2+} Complexes of C_2-Symmetric Pseudopeptides with an Aromatic Central Spacer

Lingaraju Gorla, Vicente Martí-Centelles, Lena Freimuth, Belén Altava,* M. Isabel Burguete, and Santiago V. Luis*

Departamento de Química Inorgánica y Orgánica, Universitat Jaume I, Av. de Vicent Sos Baynat, s/n, 12071, Castellón, Spain

Supporting Information

ABSTRACT: Two new tetradentate C_2-symmetric pseudopeptidic ligands derived from Val and Phe containing two amino and two amido groups and a central *o*-substituted aromatic spacer have been prepared. Their complexes with Cu^{2+}, Zn^{2+}, and Ni^{2+} have been studied by potentiometry, UV−vis spectrophotometry, FT-IR, and ESI-MS. The presence of the aromatic spacer provides Cu^{2+} complexes with stability constants several orders of magnitude higher than those observed for related ligands containing aliphatic central spacers. Besides, the formation of $[MH_{-2}L]$ complex species is favored. Crystal structures for the corresponding Cu^{2+} and Ni^{2+} have been obtained, revealing the metal atom in an essentially square-planar geometry, although, in several instances, the oxygen atom of an amide carbonyl of a second complex species can act as a fifth coordination site. In the case of Zn^{2+}, the only crystal structure obtained displays a square-pyramidal arrangement of the metal center. Finally, preliminary experiments show the catalytic activity of some of these complexes, in particular, Zn^{2+} complexes, for epoxide ring-opening with using aniline as the nucleophile in a ligand accelerated process.

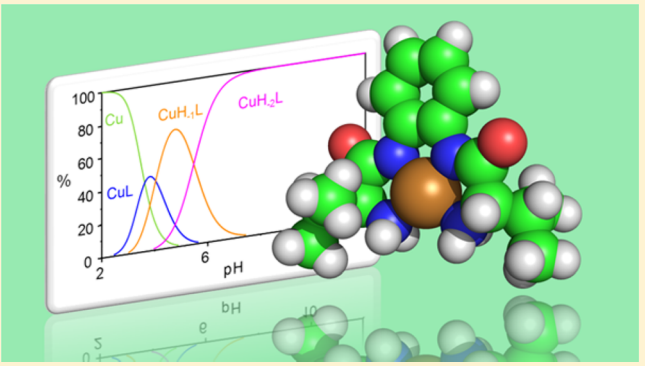

INTRODUCTION

Metal chelation is involved in many biological processes. Thus, copper is responsible for the normal function of many tissues, including immune, nervous, and cardiovascular systems.[1] Moreover, in recent years, metal-related drugs have gained much importance in medicinal chemistry. They are currently in use as medicines for the treatment of diabetes, cardiovascular diseases, and cancer and as anti-inflammatory and antimicrobial.[2−5] A large variety of ligands have been explored in coordination chemistry,[6−8] and the inclusion of amino acid residues in their structure is an important strategy, not only for their strong coordinating ability for a variety of metal ions but also because they provide coordination environments similar to those found in metalloproteins with multiple binding sites.[9] In this context, amino acid derived open-chain and macrocyclic compounds have recently drawn much attention in very different fields like synthetic,[10] bioorganic,[11] medicinal,[12] and supramolecular chemistry,[13] or in catalysis.[14] In this context, symmetrical tetracoordinated Schiff base metal complexes derived from amino acids, containing aromatic central spacers, have been studied as catalysts for Et_2Zn addition reactions and as chiral porphyrin mimics.[15] Furthermore, recent contributions from our group have shown how minimalistic pseudopeptides derived from simple natural amino acids, with the general structures I−III (Chart 1), can have important applications,[16] and have been reported as chiral solvating agents or selective receptors for substrates of biological relevance,[17] as minimalistic molecular machines,[18] as organogelators,[19] acting as "*in vivo*" fluorescent pH probes,[20] and as ligands for the preparation of enantioselective catalysts.[21]

Regarding metal complexation, our group has recently studied the coordination ability of some C_2-symmetrical bis(amino amides) derived from amino acids with the general structure I and possessing an aliphatic central spacer ($-(CH_2)_n-$) toward Cu^{2+} and Zn^{2+} ions.[22] The obtained results revealed that both the nature of the constituent amino acid (R in I) and the length of the aliphatic spacer (*n* in $-(CH_2)_n-$) were of importance in determining the complexes formed and their stability. Taking this into account, the substitution of the flexible aliphatic central spacer in I by a rigid aromatic spacer derived from *o*-diaminobenzene seems to be a logical step forward for a proper understanding of the coordination properties of this family of ligands. This aromatic spacer should not only provide a geometrically more defined coordination environment but also induce a modification of the acidity of the N−H of the amide group and, accordingly, of its involvement in the coordination to metal centers.

In this context, here we present the synthesis, characterization, and study of a family of bis(amino amide) ligands I derived from L-valine and L-phenylalanine and having an aromatic central spacer based on *o*-diaminobenzene, as well as

Received: May 2, 2016

DOI: 10.1021/acs.inorgchem.6b01066
Inorg. Chem. XXXX, XXX, XXX−XXX

Chart 1. General Structures for Pseudopeptides

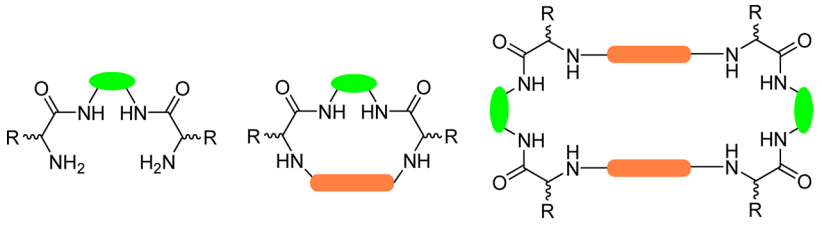

I II III

Scheme 1. Synthesis of Chiral Bis(amino amide) Ligands[a]

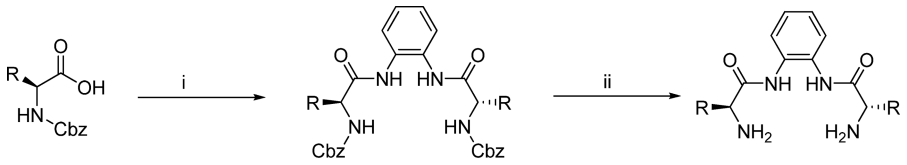

1 R = $CH(CH_3)_2$
2 R = CH_2Ph
3 R = $CH(CH_3)_2$
4 R = CH_2Ph
5 R = $CH(CH_3)_2$
6 R = CH_2Ph

[a]Reagents: (i) Et_3N, ClCOOEt, *o*-phenylenediamine, −10 °C, 2 h, then rt, 24 h, THF, 39−57%; (ii) H_2/Pd-C, MeOH, rt, 8 h, 53−66%.

Table 1. Logarithms of Stepwise Basicity Constants of Ligands 5−8 Determined at 298 K

reaction[a]	**5**[c]	**7**[d,f]	**8**[c,g]	**5**[e]	**6**[e]
H + L ⇌ HL	8.13(3)[b]	7.94(1)	7.57(1)	7.09(9)	7.17(3)
H + HL ⇌ H_2L	6.89(3)	6.96(1)	6.70(1)	7.08(9)	6.21(3)

[a]Charges omitted for clarity. [b]Values in parentheses are the standard deviations in the last significant figure. [c]0.1 M NaCl. [d]0.15 M $NaClO_4$ (ref 22a). [e]0.1 M NaCl/CH_3CN 7/3 v/v. [f]ref 22a. [g]ref 22b.

the analysis of their binding ability toward Cu^{2+}, Zn^{2+}, and Ni^{2+}. Moreover, preliminary studies on the catalytic properties of some of the complexes prepared have been carried out.

RESULTS AND DISCUSSION

Syntheses. Open-chain pseudopeptides **5** and **6** derived from L-valine and L-phenylalanine, respectively, could be easily prepared starting from the corresponding *N*-Cbz protected amino acid (**1** and **2**) through the initial formation of the corresponding *N*-protected bis(amino amide) (**3** and **4**) by reaction with *o*-phenylenediamine and its *N*-deprotection by hydrogenolysis, following previously reported procedures for related compounds (Scheme 1).[23] Overall yields for the preparation of compounds **5** and **6** after the final deprotection step were in the 53−66% range. These bis(amino amides) were fully characterized by ^1H NMR, ^{13}C NMR, FT-IR, and ESI-MS techniques (Figures S1−S6).

Acid−Base Properties. The proper determination of the acid−base properties of nitrogenated compounds is essential for understanding their coordination properties.[24,25] Thus, the protonation constants of bis(amino amides) **5** and **6** were determined by potentiometric titrations. Although compound **5** was soluble enough to carry out the corresponding studies in 0.1 M NaCl, the low solubility of **6** in this medium required the use of a mixed solvent (0.1 M NaCl/CH_3CN 7/3 v/v) for the corresponding studies. All the titrations were carried out as is fully described in the Experimental Section, at 298 K, using 0.1 M NaCl or 0.1 M NaCl/CH_3CN 7/3 v/v as the supporting electrolyte to maintain a constant ionic strength. The stepwise stability constants for the protonation of these pseudopeptidic derivatives obtained following this methodology and using the program HYPERQUAD[26] are presented in Table 1. For the potentiometric studies in 0.1 M NaCl/CH_3CN 7/3 v/v, the value used for pK_w was determined to be 14.6.[27] The constants previously obtained in 0.1 M NaCl for the related valine and phenylalanine bis(amino amides) with an ethylenic central spacer **7** and **8** (Chart 2) have also been included for comparison.[22]

Chart 2. Pseudopeptidic Ligands (7−8) Related to Compounds 5 and 6 Containing an Ethylenic Central Spacer

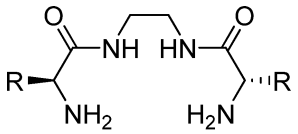

7 R = $CH(CH_3)_2$
8 R = CH_2Ph

The comparison of the constants obtained in 0.1 M NaCl for ligands **5** and **7** derived from Val reveals that the substitution of the ethylenic spacer by the aromatic one seems to have no effect on the observed basicity in water. Even in the case of the second protonation constant, the values are comparable, indicating that, in both cases, an appropriate separation of the two positive charges in the diammonium salt occurs. The change in the solvent system to 0.1 M NaCl/CH_3CN 7/3 v/v is accompanied, for ligand **5**, by a reduction in the first basicity constant of about 1 order of magnitude that does not happen for the second protonation constant. As a result, the two stepwise protonation constants for **5** are very close, which is remarkable. This can suggest that, in the nonprotonated compound, for this solvent mixture, the amino nitrogen atoms

DOI: 10.1021/acs.inorgchem.6b01066
Inorg. Chem. XXXX, XXX, XXX−XXX

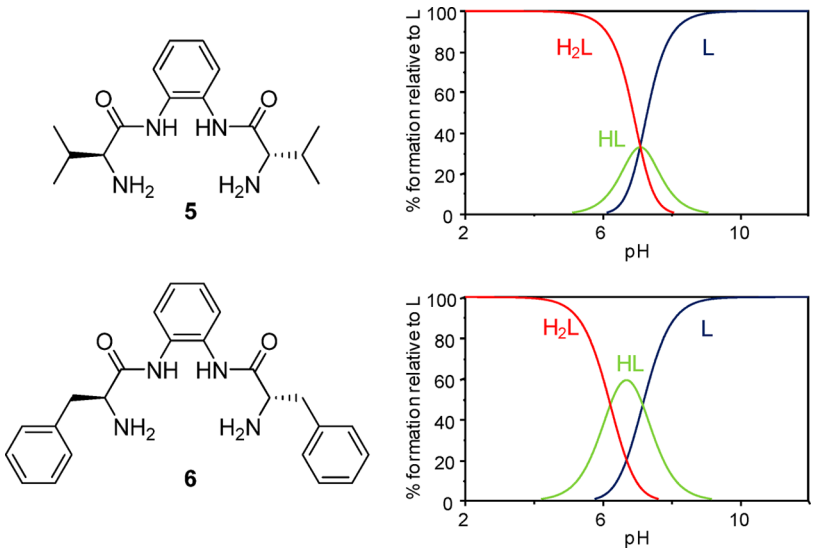

Figure 1. Distribution diagrams for the protonated species of compounds **5** and **6** (0.1 mM) as a function of pH in 0.1 M NaCl/CH_3CN 7/3 v/v at 298 K. Charges have been omitted for clarity.

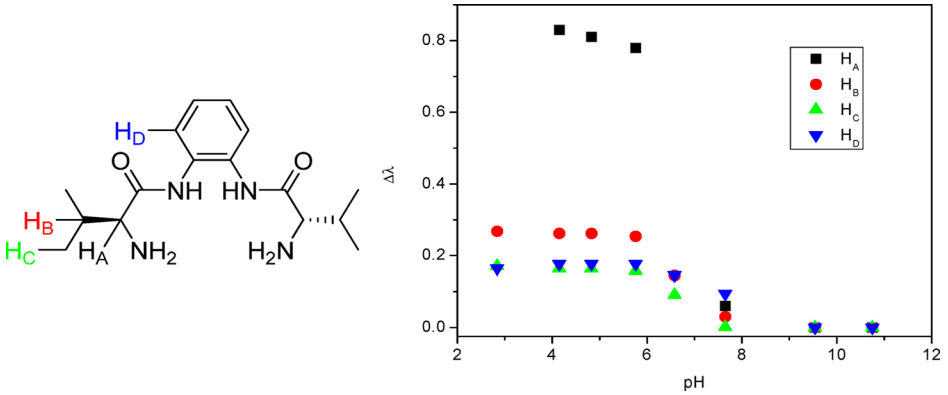

Figure 2. ^1H NMR chemical shift variation against pH for selected signals in compound **5**, 1 mM in D_2O/CD_3CN 7/3 v/v.

Table 2. Logarithms of the Formation Constants (log β) for the Cu^{2+} Complexes with Pseudopeptidic Ligands at 298 K

reaction[a]	5[c]	7[d,f]	8[c,g]	5[e]	6[e]
Cu + L ⇌ CuL	8.48(9)[b]	6.09(4)		8.83(4)	9.24(3)
Cu + L ⇌ $CuH_{-1}L$ + H		0.67(1)	1.11(1)	4.8(1)	5.03(2)
Cu + L ⇌ $CuH_{-2}L$ + 2H	0.17(1)	−6.48(1)	−6.27(1)	−0.69(3)	−0.54(3)

[a]Charges omitted for clarity. [b]Values in parentheses are the standard deviations in the last significant figure. [c]0.1 M NaCl. [d]0.15 M $NaClO_4$ (ref 22a). [e]0.1 M NaCl/CH_3CN 7/3 v/v. [f]ref 22a. [g]ref 22b.

are involved in strong hydrogen bonding that needs to be broken for the first protonation to occur. As in the case of the pseudopeptides containing an ethylenic spacer,[22] the change in the side chain from isopropyl to benzyl produces a reduction in the overall basicity of **6** relative to **5**. Most likely, this reflects the interference of the aromatic rings of the side chains with the solvation of the ammonium ions. However, the first protonation constants for **5** (log K_{H1} 7.09) and **6** (log K_{H1} 7.17) are very close, and only the second protonation constant is higher for **5** than for **6** (log K_{H2} 7.08 and 6.21, respectively). This again suggests a particular behavior of **5** in its first protonation in this solvent mixture. The importance of the amino acid side chain on the solvation and hydrogen-bonding networks has been demonstrated in the study of dynamic processes in related pseudopeptides.[18]

The distribution diagrams for **5** and **6** in the mixed solvent (Figure 1; see Figure S7 for the distribution diagram of **5** in 0.1 M NaCl) revealed the presence of HL^+ species at pH 7 for both ligands (being the major species for **6**) while H_2L^{2+} species predominate for the pH regions below 7 (ligand **5**) and 6 (ligand **6**), being the only species present below pH 5 and 4, respectively. Neutral L species start to predominate for both ligands at pH > 7.

The protonation of ligand **5** was also monitored by ^1H NMR spectroscopy,[28] using a solvent mixture similar to the one used for potentiometric titrations (ligand **5**, 1 mM in D_2O/CD_3CN 7/3 v/v) (see Figure S8). Although the signal for the hydrogen atom at the chiral carbon atom partly overlaps with the water solvent signal at pH regions close to 7, this signal experiments a significant downfield shift between pH 8 and pH 6 ($\Delta\delta$ > 0.7 ppm), in good agreement with potentiometric data. Moreover,

DOI: 10.1021/acs.inorgchem.6b01066
Inorg. Chem. XXXX, XXX, XXX−XXX

Table 3. Logarithms of the Formation Constants (log β) for the Complexes of Zn^{2+} with Pseudopeptidic Ligands at 298 K

reaction[a]	5[c]	7[d]	5[e]	6[e]
Zn + L ⇌ ZnL			4.05(1)	3.81(4)
Zn + L ⇌ $ZnH_{-2}L$ + 2H	−12.22(8)[b]	−12.44(1)	−10.01(1)	−10.45(3)

[a]Charges omitted for clarity. [b]Values in parentheses are the standard deviations in the last significant figure. [c]0.1 M NaCl. [d]0.15 M $NaClO_4$ (ref 22a). [e]0.1 M NaCl/CH_3CN 7/3 v/v.

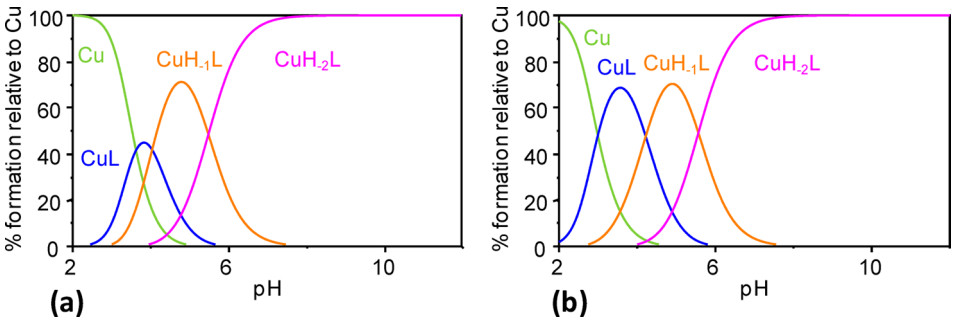

Figure 3. Distribution diagrams for ligands **5** (a) and **6** (b) with Cu^{2+} as a function of pH in 0.1 M NaCl/CH_3CN 7/3 v/v, at 298 K. Charges have been omitted for clarity. [L] = [Cu^{2+}] = 0.1 mM.

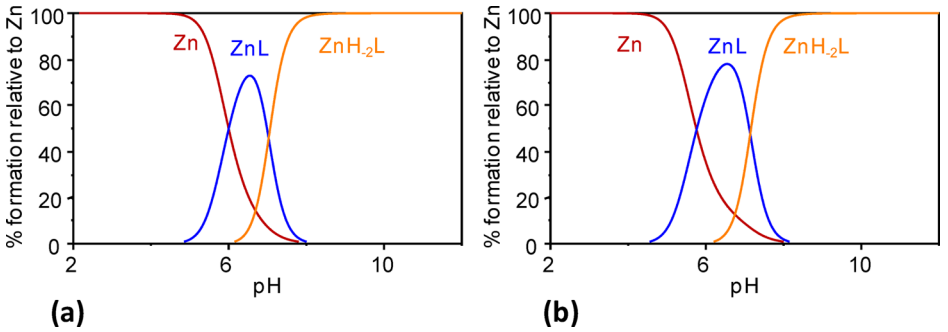

Figure 4. Distribution diagrams for ligands **5** (a) and **6** (b) with Zn^{2+} as a function of pH in 0.1 M NaCl/CH_3CN 7/3 v/v, at 298 K. Charges have been omitted for clarity. [L] = [Zn^{2+}] = 0.1 mM.

similar trends are observed for the shifts of other signals as shown in Figure 2.

Determination of the Cu^{2+} and Zn^{2+} Complexes Formation Constants. Because of the interest in developing metal-containing model systems for metalloproteins, and taking into account our previous experience in this field, the copper, zinc, and nickel complexes of the new ligands were investigated to explore their coordination chemistry. The interaction of ligands **5** and **6** with Cu^{2+} and Zn^{2+} was studied by potentiometric titrations in 0.1 M NaCl and 0.1 M NaCl/CH_3CN 7/3 v/v over the 2−12 pH range at 298 K. The stability constants for the formation of complexes were determined for a 1:1 metal−ligand ratio. As in the case of the protonation constants, accurate results for **6** could only be obtained in the mixed solvent because of its limited solubility in water. Results obtained are presented in Tables 2 and 3, and the corresponding distribution diagrams are displayed in Figures 3 and 4. The values obtained previously for the related ligands **7** and **8** have also been included for comparison.[22a]

As seen in Table 2, the comparison between ligands **5** and **7** in 0.1 M NaCl highlights the importance of the central spacer. The stability of the complexes detected is several orders of magnitude higher in the case of the ligand with the central aromatic spacer (**5**). Moreover, for **5**, only two complex species (nondeprotonated and bisdeprotonated) were detected, while the monodeprotonated $[CuH_{-1}L]^+$ species was also detected for **7**, being present at pH regions around neutrality.[22a] In this regard, the corresponding distribution diagrams differ significantly and the relative importance of the neutral $[CuH_{-2}L]$ species was very different (Figure S9 for the distribution diagram of **5** with Cu^{2+} in 0.1 M NaCl). For **7**, this complex species starts to be formed at pH values slightly below 6, becoming the major species in the basic region from *ca.* pH > 7. On the contrary, for **5**, the $[CuH_{-2}L]$ species is formed at pH values slightly below 4 and becomes predominant above pH 4. For compound **5**, the free cation is only the major species at the very acidic regions below pH 4, while for **7** predominates below pH 6.[22a]

As mentioned above, the comparison of **5** and **6** required a mixed solvent (0.1 M NaCl/CH_3CN 7/3 v/v). When comparing the data for **5** in both solvents, it can be observed that the dicationic complex $[CuL]^{2+}$ is slightly more stable in the mixed solvent, but the neutral complex $[CuH_{-2}L]$ is 1 order of magnitude less stable. This can be associated with the presence of CH_3CN in the solvent mixture that could participate to a higher extent in the coordination to the $[CuL]^{2+}$ species. On the other hand, the mixed solvent can reduce the basicity of the amide groups. This allows the observation of $[CuH_{-1}L]^+$ as an important species that becomes predominant at *ca.* pH 5.5 (Figure 3). In any case, the values of the stability constants continue being several orders of magnitude higher than those measured for ligand **7**,

DOI: 10.1021/acs.inorgchem.6b01066
Inorg. Chem. XXXX, XXX, XXX−XXX

containing a central ethylenic spacer, in water. In this mixed solvent, the values of the formation constants were slightly lower for ligand **5** (i.e., log K = 8.83 and 9.24, respectively, for $[CuL]^{2+}$), which can reflect similar phenomena than in the case of the protonation constants. The corresponding distribution diagrams (Figure 3) display similar trends for both ligands and are in line with the distribution diagram observed for **5** in 0.1 M NaCl (Figure S9) except for the presence of the $[CuH_{-1}L]^{+}$ complex species that predominate around pH 5. Thus, the $[CuH_{-2}L]$ species start to be formed at pH values above 4 and become the major species above pH 6. On the other hand, the $[CuL]$ species are present at pH values around 4 and are particularly relevant for ligand **6**. According to this, free Cu^{2+} species are only predominant at the very acidic pH regions, below pH 3.5 for **5** and below pH 3 for **6**.

A similar study was carried out in the case of the Zn^{2+} cation (Table 3). As has been observed for most nitrogenated ligands and in particular for those related to **5** and **6**, the Zn^{2+} complexes are significantly less stable than those for Cu^{2+} with formation constants several orders of magnitude lower. In this case, no appreciable differences were obtained as a consequence of the change in the central spacer. Similar values were calculated in water for the formation constants of the $[ZnH_{-2}L]$ species for **5** and **7**, being this one the only complex species detected. The corresponding distribution diagrams were also very similar, with the neutral complex species being formed at basic pH values and becoming the major species at about pH 8 (Figure S9).[22a]

In the mixed solvent, ligands **5** and **6** displayed a very similar behavior, with the formation of $[ZnL]$ and $[ZnH_{-2}L]$ complex species. Interestingly, $[ZnL]$ species are only detected in this medium, revealing a higher stability of these complexes. The formation constants observed for the $[ZnH_{-2}L]$ species are 2 orders of magnitude greater in this medium. This trend separates from the one observed for copper complexes and most likely can be related to the specific behavior of Zn^{2+} in water. The corresponding distribution diagrams are shown in Figure 4. For both ligands, the neutral complexes $[ZnH_{-2}L]$ start to be formed at pH values above 6 and become the dominant species in both systems at pH > 7.5, while the $[ZnL]^{2+}$ species predominate at neutrality and the Zn^{2+} ion starts to be the dominant zinc species slightly below pH 6. The slow kinetics usually associated with Ni^{2+} complexes hindered their study by potentiometric techniques.

Spectroscopic and Mass Spectrometry Studies. The $[MH_{-2}L]$ complexes of **5** and **6** with Cu^{2+}, Zn^{2+}, and Ni^{2+} were synthesized in MeOH with the addition of 2 equiv of KOH (Scheme 2). The process was accompanied by a change in color from blue to purple for the two Cu^{2+} complexes and from green to yellow for the Ni^{2+} complexes, while, as could be expected, colorless complexes were formed in the case of Zn^{2+}. Moreover, their formation could be followed by FT-IR experiments by a significant shift of the C═O band to lower frequencies (i.e., 1551 cm^{-1} for **9a** against 1661 cm^{-1} for **5**, Figure S10), confirming the deprotonation of the amide group.[22]

Scheme 2. Synthesis of Metal Complexes Derived from Bis(amino amides) 5 and 6

In order to gain a more detailed insight into the nature of the metal complexes formed with ligands **5** and **6**, UV–vis spectroscopic studies were carried out, in the case of Cu^{2+}, by selecting preferentially those pH regions at which one of the complex species is dominant. For this purpose, the pH of a 0.1 mM solution (50 mL) of the ligand and $Cu(OAc)_2$ in 0.1 M $NaCl/CH_3CN$ 7/3 v/v was adjusted to *ca.* 2 by the addition of 50 μL of concentrated HCl. This sample was titrated exactly under the same conditions used for the potentiometric titrations described above using a 0.1 M NaOH solution in water. Aliquots of 2 mL were taken for UV–vis analysis at the selected pH values, and the resulting spectra are presented in Figure 5a,b. In the more acidic pH regions where the presence of $[CuL]^{2+}$ or the uncomplexed cation is relevant, an ill-defined broad band with the maximum above 700 nm is observed. This band has been traditionally assigned to the d–d transitions associated with octahedral Cu^{2+} complexes, although different data suggest that free Cu^{2+} can be pentacoordinated instead of hexacoordinated.[29a] In this context, it is important to bear in mind that currently there is a strong debate of the actual coordination number (five-coordinated or six-coordinated) of many Cu^{2+} complex species of different nature.[29] This band is more clearly visible for ligand **5** in MeOH (Figure 5c), displaying at acidic pH values an intense band with its maximum above 800 nm (i.e., 880 nm at pH 1.6). The formation of deprotonated $[CuH_{-x}L]$ complexes is accompanied by an important bathochromic shift for this transition that appears as an intense band slightly above 500 nm (at pH > 10, 505, and 510 nm for **5** and **6**, respectively). This is in good agreement with the predominance of square-planar or square-pyramidal geometries.[15,30]

The complex species formed by **5** and **6** with Cu^{2+} and Zn^{2+} were also studied by mass spectrometry in methanol at the acidic and basic regions. Again, the slow kinetics associated with Ni^{2+} precluded an appropriate study of the corresponding complexes. The ESI-MS technique allows the detection in a solution of species at low concentration, and this makes it attractive to analyze complexation processes.[31] This confirmed the formation of deprotonated complex species even at acidic pH regions. Thus, for instance, the ESI-MS spectrum, in the positive mode of analysis, of the Cu^{2+}-**5** system at pH 4 showed a major peak corresponding to $[\mathbf{5} + H]^{+}$ at 307 and a peak at 368 corresponding to the one expected for the $[CuH_{-1}L]^{+}$ species. Full isotopic analysis showed a perfect agreement between simulated and experimental mass spectra (Figure S11). It must be noted that the peak at 368 can also correspond to the ion $[CuH_{-2}L + H]^{+}$ taking into consideration that the $[CuH_{-2}L]$ species is neutral and for being observed in the ESI-MS^{+} mode requires the interaction with an additional positively charged species (H^{+}, Na^{+}, K^{+}, or other species depending on experimental conditions). This was confirmed by the observation of a smaller peak, with the correct isotopic pattern, at 406 corresponding to the $[CuH_{-2}L + K]^{+}$ species.

The observation of the bisdeprotonated complex species $[MH_{-2}L]^{+}$ is easier at basic pH values. Thus, for Zn^{2+}

DOI: 10.1021/acs.inorgchem.6b01066
Inorg. Chem. XXXX, XXX, XXX–XXX

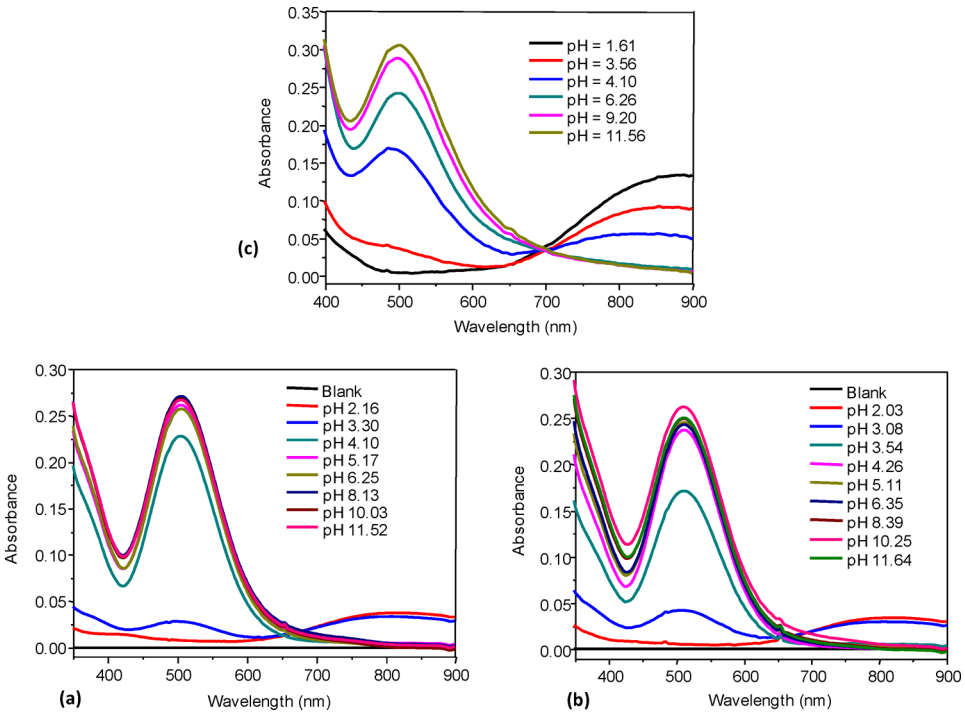

Figure 5. UV−vis spectra in 0.1 M NaCl/CH_3CN 7/3 v/v for the systems: (a) Cu^{2+}-**5**, (b) Cu^{2+}-**6**, and (c) for Cu^{2+}-**5** in MeOH (*ca.* 0.1 mM in the ligand and in $Cu(OAc)_2$) at different pH values.

Table 4. Selected Bond Distances and Angles for Metal Complexes 9a−c and 10a,c

complex	M−N distance (Å)	molecule A	molecule B	N−M−N angle	molecule A	molecule B
9a	Cu1−N1	1.985	2.004	N1−Cu1−N2	107.2	106.8
9a	Cu1−N2	2.013	1.979	N2−Cu1−N4	83.7	84.8
9a	Cu1−N3	1.912	1.905	N3−Cu1−N4	84.3	84.3
9a	Cu1−N4	1.918	1.907	N3−Cu1−N1	84.8	84.2
9b	Zn1−N1	2.124		N1−Zn1−N2	102.8	
9b	Zn1−N2	2.123		N2−Zn1−N4	79.2	
9b	Zn1−N3	2.062		N3−Zn1−N4	78.9	
9b	Zn1−N4	2.039		N3−Zn1−N1	79.7	
9c	Ni1−N1	1.915	1.912	N1−Ni1−N2	100.3	101.2
9c	Ni1−N2	1.906	1.921	N1−Ni1−N3	86.5	85.9
9c	Ni1−N3	1.833	1.827	N3−Ni1−N4	86.6	86.3
9c	Ni1−N4	1.827	1.827	N4−Ni1−N2	86.5	86.6
10a	Cu1−N1	2.004	1.990	N1−Cu1−N2	108.57	105.5
10a	Cu1−N2	2.023	2.005	N1−Cu1−N3	84.63	85.1
10a	Cu1−N3	1.918	1.907	N3−Cu1−N4	83.67	84.5
10a	Cu1−N4	1.922	1.899	N4−Cu1−N2	83.48	84.8
10c	Ni1−N1	1.909		N1−Ni1−N3	86.66	
10c	Ni1−N3	1.829		N3−Ni1−N3	86.44	
10c				N1−Ni1−N1	100.28	

complexes formed with **5**, the ESI-MS^+ measured at pH 9.1 showed a peak at 345 corresponding to $[\mathbf{5} + K]^+$ and a peak at 407 corresponding to the $[ZnH_{-2}L + K]^+$ species (Figure S11). Peaks with the correct isotopic pattern were also observed at 439 and 505 corresponding to the formation of the $[ZnH_{-2}L + K + CH_3OH]^+$ and $[ZnH_{-2}L + K + 2NaOH + H_2O]^+$ clusters.

Single-Crystal X-ray Diffraction Studies. The presence of the rigid aromatic central spacer significantly enhanced the possibility of obtaining crystals of good quality for diffraction studies. In many instances, crystals were formed directly in the samples obtained from potentiometric titrations at basic pH values. X-ray quality single crystals for the complexes were grown by layering an ethanolic solution of the pseudopeptidic ligand over an aqueous solution of $Cu(OAc)_2$, $Zn(OAc)_2$, and $Ni(OAc)_2$, respectively. Thus, suitable crystals for X-ray diffraction analysis were obtained, in the case of ligand **5**, for the three $[MH_{-2}L]$ complexes **9a−c**. For ligand **6**, appropriate crystals were obtained for the ligand itself and for its Cu^{2+} and Ni^{2+} complexes, **10a**, and **10c**. For the $[MH_{-2}L]$ complexes, the main features of the corresponding X-ray structures are shown in Table 4 (see also Tables S1, S2, and S4−S7).

The crystallographic structure for the free ligand **6** is shown in Figure 6 (see also Tables S2 and S3). Four independent molecules (A−D) participate in the asymmetric unit. The

DOI: 10.1021/acs.inorgchem.6b01066
Inorg. Chem. XXXX, XXX, XXX−XXX

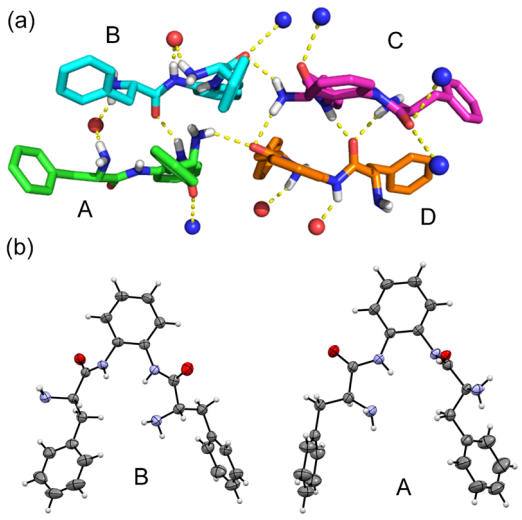

Figure 6. Schematic representation of the hydrogen bond network in the packing of the free ligand **6** (a) and the molecular structure of the two conformations present for ligand **6** (b).

presence of the aromatic central unit preorganizes the molecules in U-shaped conformations. Molecules B and C have the corresponding U-shapes aligned in the same direction, while molecules A and D are oriented in the opposite direction. Two main conformations are observed. For molecules A and D, one of the amide groups is coplanar with the central aromatic ring (8.8° C−C−N−H torsion angle) and the second one is almost perpendicular (83.1° and 91.1° C−C−N−H torsion angles for A and D, respectively). In molecules B and C, none of the amide groups is coplanar with the aromatic ring, defining torsion angles ranging from 31.9° to 56.5°. All the amide groups display the expected almost perfect anticoplanar arrangement with O−C−N−H torsion angles between 170.8° and 177.9°. Amide N−H fragments are always oriented toward the cavity defined by the molecular cleft, facilitating the convergence of the nitrogen atoms (three for B and C and the four for A and D) on this cleft.[32] This also favors the participation of the oxygen atoms of the carbonyl groups in the formation of an extensive network of intermolecular hydrogen bonding, in particular, in the case of molecules B and C for which the two amide groups show an antidisposition in two planes displaying 33.8° and 37° angles, leading to the formation of hydrogen bonds with adjacent molecules located in opposite directions. Besides, the aromatic groups of the side chains display edge-to-face arrangements with neighboring aromatic rings from other side chains or from the central spacer. These $\pi-\pi$ interactions are characterized by the presence of H···C_{ar} distances < 3 Å (up to 2.86 Å) representing $\%vd_{W}H,C < 100$.[33]

In the case of the [$CuH_{-2}L$] complex formed by ligand **5** (**9a**), two [$CuH_{-2}L$] units form the asymmetric unit in the crystalline structure (Figure 7a). In one of those units, the coordination environment around the copper presents a slightly distorted square-pyramidal geometry in which the square base is formed by the four nitrogen atoms of a bisdeprotonated ligand. The oxygen atom from a carbonyl group of the second molecule provides the fifth axial coordination, being the Cu−O distance (2.663 Å) significantly longer that those corresponding to Cu−N distances that range from 1.912 to 2.013 Å. The copper atom is essentially located in the plane defined by the four nitrogen atoms, although a small distortion is observed with the Cu-plane distance being 0.047 Å. The O−Cu−N angles defined are 82.3° and 82.7° for the amide nitrogen atoms and 104.2° and 100.6° for the amino nitrogen atoms. The bite angles for the five chelate rings range from 83.7° to 84.8°, indicative of a tight chelation. In concordance, the N_{amine}−Cu−N_{amine} bite angle is 107.2°. The coordination geometry around the Cu^{2+} for the second molecule is square-planar, with the copper atom located at 0.015 Å from the plane defined by the four nitrogen atoms. In this case, the Cu−N distances range from 1.905 to 2.004 Å, slightly shorter as could be expected from the absence of the fifth donor atom. The bite angles for the five chelate rings range from 84.2° to 84.8°, in this case, with the N_{amine}−Cu−N_{amine} bite angle being 106.7°. In both molecules, the Cu−N_{amide} distances are shorter than the ones corresponding Cu−N_{amine}, being 1.911 and 1.995 Å on average, respectively. The latter was previously observed for analogous Cu−pseudopeptidic complexes and was attributed to the anionic coordination from the deprotonated N_{amide} donors instead of the neutral donation from the N_{amine} groups.[22b]

The unit cell for complex **9a** contains four of such pairs of [$CuH_{-2}L$] units, and besides, two water molecules are present for each [$CuH_{-2}L$] unit. These water molecules play a key role

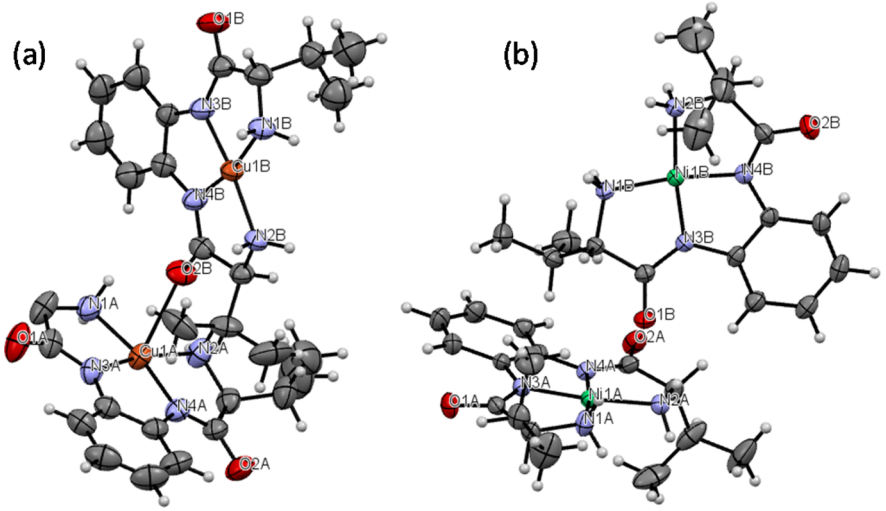

Figure 7. Molecular structure for complexes **9a** (a) and **9c** (b) in their crystal structures.

DOI: 10.1021/acs.inorgchem.6b01066
Inorg. Chem. XXXX, XXX, XXX−XXX

in the hydrogen-bonding network present in the crystal structure (Figure S12). For the [CuH$_{-2}$L] unit containing the square-pyramidal copper ion, each of the oxygen atoms of the deprotonated amide groups acts as hydrogen bond acceptor with one molecule of water and one amino group of a different molecule and only one of its amino groups acts as a hydrogen donor with a third water molecule. For the square-planar [CuH$_{-2}$L] unit, the noncoordinated amide carbonyl is hydrogen bonded to a water molecule while the amino groups form hydrogen bonds with the oxygen atoms from the amide groups of two different molecules and one of them also acts as hydrogen donor with a water molecule.

The crystal structure of the Ni^{2+} complex with the bisdeprotonated ligand **5** (**9c**) displays some common features with the one analyzed for the Cu^{2+} complex **9a**. The asymmetric unit for complex **9c** (Figure 7b) is also formed by two [NiH$_{-2}$L] units defining almost perpendicular main planes (87.6°). In one of these units, the nickel presents an almost perfect square-planar geometry. The four Ni−N distances are 1.827 Å for both Ni−N$_{amide}$ and 1.912 and 1.921 Å for Ni−N$_{amine}$. The three bite angles for the chelate rings are very close to 86°, higher than in the case of Cu^{2+}. The Ni atom is located at 0.013 Å from the plane defined by the nitrogen atoms. In the second [NiH$_{-2}$L] unit, the nickel atom displays a more distorted square-planar geometry becoming intermediate with the one for a square-pyramidal coordination. In this regard, the oxygen atom of one amide group of the other unit is located at 2.970 Å from the nickel atom. Besides this long distance, it must be noted that the oxygen atom is significantly displaced from the vertical, defining OCuN angles of 100.9° and 109.8° for the amide nitrogen atoms and 69.1° and 78.4° for the amino nitrogen atoms. The unit cell for complex **9c** contains eight [NiH$_{-2}$L] units, grouped in four pairs, and eight water molecules. Moreover, an extensive network of intermolecular hydrogen-bonding interactions can be observed between the O atoms of the carbonyl groups and the H atom of the amine groups and/or the water molecules. The amino groups also participate as hydrogen bond donors with water molecules (Figure S13).

In the case of the Zn complex (**9b**), only one [ZnH$_{-2}$L] species contributes to the asymmetric unit (Figure 8) along with a molecule of isopropanol. In the corresponding molecular structure, the Zn atom displays a distorted square-pyramidal geometry in which the square base is formed by the terminal amine and the deprotonated amide nitrogen atoms of the ligand **6**. The oxygen atom from the carbonyl group of a second molecule occupies the apical coordination position of the square-pyramidal geometry. The metal center lies above the mean plane of the coordinated nitrogens by 0.603 Å. The Zn−N$_{amine}$ distances average 2.123 Å and the Zn−N$_{amide}$ 2.051 Å, being the Zn−O distance 1.996 Å. The distortion in the square-pyramidal geometry is clearly reflected in the O−Zn−N angles present. The two angles involving the N$_{amide}$ atoms are 116.1° and 114.4°, while the two involving the N$_{amine}$ atoms are 99.5° and 100.3°. The bite angles for the three chelate rings are very similar and slightly below 80° (79.7°, 79.2°, and 78.9°), providing a N$_{amine}$−Cu−N$_{amine}$ bite angle of 102.8°. Four independent [ZnH$_{-2}$L] units and four *i*-PrOH molecules define the unit cell. The association of contiguous [ZnH$_{-2}$L] units through O−Zn bonds provides the formation of unidimensional polymeric chains. The contiguous units are not parallel, but their main plains, as defined by the aromatic carbons and the four nitrogen atoms, are tilted by *ca.* 41° and the aromatic

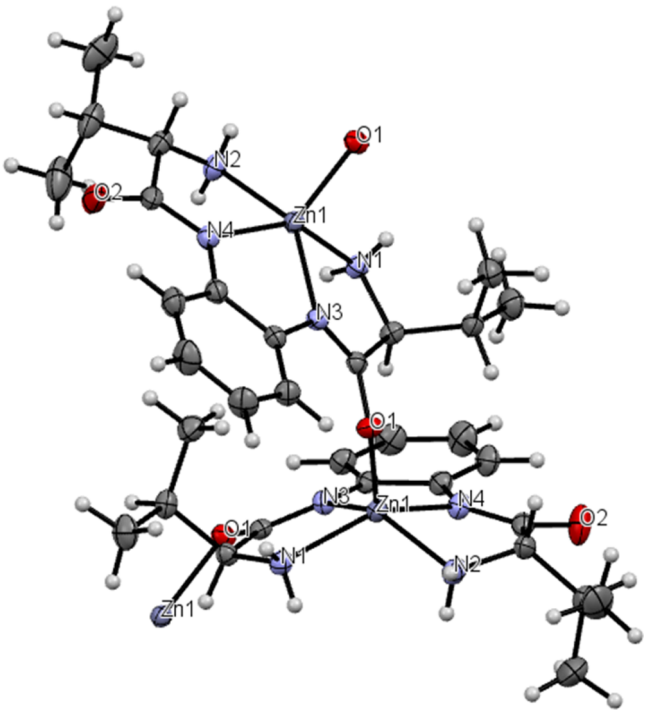

Figure 8. Molecular structure for complex **9b**. The arrangement of two consecutive molecular units is displayed to highlight the interaction of the oxygen atom of one amide of the first [ZnH$_{-2}$L] unit with the Zn atom of the second one.

fragments are located at opposite sites. The *i*-PrOH molecules play a key role in defining the intermolecular interactions leading to the stabilization of the three-dimensional structure observed in the crystal packing. Each *i*-PrOH molecule acts as hydrogen bond acceptor with one hydrogen atom of the NH_2 group closer to the carbonyl group bound to Zn (NH···O distance 2.189 Å) of a [ZnH$_{-2}$L] unit and is also within a short distance of one hydrogen atom of the second NH_2 group of the same unit (2.390 Å). Besides, it acts as a hydrogen bond donor with the oxygen atom of the amide carbonyl not bound to Zn of a [ZnH$_{-2}$L] unit belonging to a second chain. As *i*-PrOH molecules associated with consecutive units are located at opposite sides of the chain, this defines a 3D hydrogen bond network (Figure S14).

The effect of the substitution of the valine fragment by the one corresponding to phenylalanine can be analyzed comparing the molecular structures of complexes **9a** and **10a** (Figures 7a and 9a). Also, in the case of **10a**, two [CuH$_{-2}$L] units are

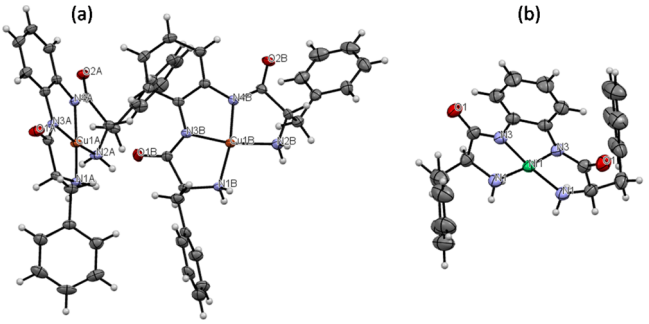

Figure 9. Molecular structure for complexes **10a** (a) and **10c** (b) in their crystal structures.

DOI: 10.1021/acs.inorgchem.6b01066
Inorg. Chem. XXXX, XXX, XXX−XXX

involved in the asymmetric unit (Figure 9a). The coordination environments of the two copper ions are very similar to those described in **9a**, with the metal coordinated to the four nitrogen atoms of ligand **6** in a formal square-planar geometry.

Again, the Cu−N_{amide} distances are slightly shorter than these for Cu−N_{amine}, being 2.006 and 1.912 Å on average, respectively. Bite angles are very similar to those found in **9a**. Also, in this case, one of the carbonyl groups of one molecule is oriented toward the metal center of the second one, suggesting an actual five coordinated distorted square-pyramidal arrangement. Nevertheless, the resulting Cu−O distance is significantly larger now (2.835 vs. 2.663 Å) and the disposition is similar to that found for the Cu^{2+} complex of the Phegly-derived ligand containing an ethylenic central spacer.[22b] The square-planar geometry is essentially coplanar with the aromatic central spacer with the angles between the corresponding mean planes being 1.4° and 7.5° in both units. The two deprotonated amide moieties are more coplanar in **10a** than in **9a**, with angles between their mean planes of 4.3° and 7.2° instead of the values of 14.6° and 18.5° found in **9a**. The presence of the additional aromatic units in **10a** is important to define the resulting packing (Figure S15). The dispositions of the two [$CuH_{-2}L$] units of the asymmetric unit are different in **9a** and **10a**. In **10a**, the two central aromatic spacers and the aromatic unit of one side chain converge, displaying edge-to-face dispositions in which the shorter H−C distances are 3.137 and 3.148 Å between the central spacers and 2.977 and 3.072 Å between the aromatic side chain and the central spacer of the second molecule (in this case, the shorter H−centroid distance is 2.984 Å).

The change in the component amino acid is more relevant in the crystal structure of the corresponding Ni^{2+} complexes. For complex **10c**, all the [$NiH_{-2}L$] units present the same molecular structure displaying a perfect C_2 symmetry (Figure 9b). As a matter of fact, only half a unit is required to define the asymmetric unit, with the unit cell involving five [$NiH_{-2}L$] structures (Figure S16). The coordination environment around the nickel shows a perfect square-planar geometry with the Ni atom in the plane defined by the four nitrogen atoms (Ni−plane distance is 0.000 Å) and Ni−N_{amide} and Ni−N_{amine} distances being 1.829 and 1.909 Å, respectively. Bite angles are very similar to those found in **9c**. The aromatic ring of the spacer and the four nitrogen atoms, along with the metal center, define essentially a single plane (deviation is 1.2°). In the molecular structure, the two aromatic rings of the side chains partly cover the space above and below the plane defined by the four nitrogen atoms and the Ni and this seem to preclude a close approaching of an additional [$NiH_{-2}L$] unit as to allow the additional coordination of the oxygen of one amide carbonyl to the metal, as observed in **9c**. In the packing, each [$NiH_{-2}L$] unit has two additional units located close to its NH_2 fragments, displaying NH···O distances of 2.387 Å. The main plain of both molecules is almost perpendicular to the one of the first unit (85.9°), one being located above this plane and the second one located below and maintaining the C_2 symmetry defined by the C_2 axis of the first [$NiH_{-2}L$] unit. Aromatic interactions are important. Each of the aromatic rings of the side chain of this first unit shows an edge-to-face arrangement with the central aromatic spacer one of these contiguous units with the $C_{ar}H\cdots C_{ar}$ shorter distance being 2.853 Å. This aromatic side chain also shows a displaced face-to-face arrangement with one of the aromatic side chains of the same molecule with the $C_{ar}H\cdots$Centroid shorter distance being 3.434 Å.

Catalytic Studies. Different metal complexes of pseudopeptidic ligands have shown to be catalytically active for a variety of organic transformations.[14,15,21,34] In this regard, the ring-opening of epoxides with an amine as the nucleophile is an important, but challenging, route for the synthesis of β-amino alcohols.[35,36] Some of the existing methods have limitations, including the failure of less basic amines to open epoxides under ambient conditions, the requirement of high catalyst loading, the need of using air- and moisture-sensitive catalysts, nonenvironmentally friendly solvents, or long reaction times.[37] Taking this into account and in order to obtain information on the potential catalytic activity of the considered metal complexes, preliminary studies were carried out on the use of the corresponding Cu^{2+}, Zn^{2+}, and Ni^{2+} complexes with ligands **5** and **6** for the ring-opening of cyclohexene oxide with aniline using water and EtOH as environmentally friendly solvents (Scheme 3).[38]

Scheme 3. Epoxide Ring-Opening Reaction Studied

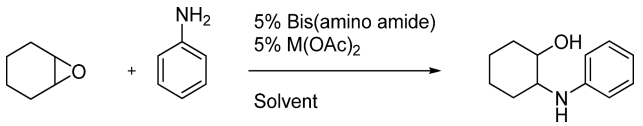

The results obtained are summarized in Table 5. In general, better yields were obtained using water as a solvent. It must be noted that, in water, the background reaction in the absence of any catalyst is relatively important (entry 20).[35b] The addition of $Zn(OAc)_2$ slightly accelerates this reaction (entry 14), but on the contrary, the addition of $Cu(OAc)_2$ seems to inhibit the process (entry 13), most likely through the strong coordination of copper to the amino groups. The addition of $Ni(OAc)_2$

Table 5. Yields Obtained in the Epoxide Ring-Opening Reaction between Cyclohexene Oxide and Aniline[a]

entry	ligand	metal	solvent	yield[b]
1	**5**	$Cu(OAc)_2$	EtOH	12.2
2	**5**	$Cu(OAc)_2$	H_2O	33.5
3	**6**	$Cu(OAc)_2$	EtOH	26.6
4	**6**	$Cu(OAc)_2$	H_2O	54.4
5	**5**	$Zn(OAc)_2$	EtOH	30.8
6	**5**	$Zn(OAc)_2$	H_2O	56.8
7	**6**	$Zn(OAc)_2$	EtOH	25.3
8	**6**	$Zn(OAc)_2$	H_2O	81.4
9	**5**	$Ni(OAc)_2$	EtOH	46.8
10	**5**	$Ni(OAc)_2$	H_2O	69.6
11	**6**	$Ni(OAc)_2$	EtOH	18.4
12	**6**	$Ni(OAc)_2$	H_2O	65.6
13		$Cu(OAc)_2$	H_2O	5.6
14		$Zn(OAc)_2$	H_2O	34.9
15		$Ni(OAc)_2$	H_2O	64.9
16		$Cu(OAc)_2$	EtOH	3.9
17		$Zn(OAc)_2$	EtOH	15.7
18		$Ni(OAc)_2$	EtOH	4.1
19			EtOH	15.9
20			H_2O	26.2

[a]Reaction conditions: 5 mol % of ligand and 5 mol % of $M(OAc)_2$, 16 h, rt. [b]Isolated yields.

DOI: 10.1021/acs.inorgchem.6b01066
Inorg. Chem. XXXX, XXX, XXX−XXX

accelerates the process to a significant extent. The formation of the corresponding complexes with ligands **5** and **6** led to an acceleration of the reaction for both Zn^{2+} and Cu^{2+} complexes, while for Ni^{2+} complexes seem to have no effect. Again the slow kinetics observed for the formation of nickel complexes can be important in this regard. This is interesting for future applications as reveals this to be a ligand accelerated process for copper and zinc complexes. In any case, copper complexes were less active than zinc complexes. For both metals, complexes formed with ligand **6** derived from Phe were more active than those from ligand **5** derived from Val (compare entries 2 and 4, 6 and 8). The best results were obtained using ligand **6** and $Zn(OAc)_2$ (81.4% yield, entry 8). Unfortunately, no enantiomeric excesses were detected in any case. Though, as mentioned above, the number of reports regarding the opening of epoxides by amines is quite limited, the present results are comparable or even better, in terms of activity, than results previously reported for the opening of cyclohexane oxide with aniline. Thus, for instance, the use of *n*-Bu_3P as catalyst has been reported to afford a 78% of the amino alcohol after 12 h using a 10% loading of phosphine, and related results were obtained with the addition of tertiary amines.[39] To analyze those results, however, it is very important to understand the crucial role played by the pH of the aqueous medium for this reaction, basic conditions favoring the process: 45 h is required at pH 7, in the absence of catalyst, to obtain a 90% yield at 30 °C, whereas just 25 h is required, for the same yield, at pH = 8.[35b] In this regard, it is worth mentioning that pH values in the 6−7 range were always obtained, in our case, for the experiments in Table 5. The use of metal complexes has been explored using Lewis acid−surfactant-combined catalysts, but this has been preferentially applied to the opening of highly hydrophobic epoxides particularly well suited for this approach.[40] In this case, for instance, using a combination of $Zn(OTf)_2$ (10%), dodecyl sulfate (10%), and a bipyridine ligand (12%), a 97% yield was obtained after 22 h, being the yield lower with copper, while nickel was essentially inactive, in line with the differences observed in our case when changing the metal. Significant decreases in catalytic activity were observed upon reduction of the catalyst loading or the concentration, best results being obtained with the use of Sc^{3+}.[40a]

CONCLUSIONS

The substitution of an aliphatic central spacer by an aromatic spacer derived from *o*-diaminobenzene in pseudopetidic structures I affords tetradentate ligands **5** and **6**, providing some interesting properties in their interaction with Cu^{2+}, Zn^{2+}, and Ni^{2+}. Potentiometric studies reveal that the stability of the complexes formed with Cu^{2+} is several orders of magnitude higher when compared to those formed by the related ligand containing an ethylenic central spacer. This is particularly relevant for the formation of the $[CuH_{-2}L]$ species, leading, as shown in the corresponding distribution diagrams, to the formation of such species even in relatively acidic regions. The preorganization of the ligands in a U-shaped conformation favored by the *o*-substitution of the aromatic spacer and the increase in acidity of the amido groups bound to the aromatic fragments can be responsible for this behavior. The differences are, however, less relevant for Zn^{2+} complexes. The rigidity of the central aromatic spacer also seems to facilitate obtaining crystals suitable for X-ray diffraction. Crystal structures for ligand **6** and $[MH_{-2}L]$ complexes Cu-**5** (**9a**), Cu-**6** (**10a**), Zn-**5** (**9b**), Ni-**5** (**9c**), and Ni-**6** (**10c**) were obtained. In the case of Cu^{2+} and Ni^{2+}, the square-planar geometry dominates, with the metal located essentially in the plane defined by the four nitrogen atoms of the ligand. This square-planar geometry is in agreement with the spectroscopic data obtained in solution for the Cu^{2+} complexes. In most cases, however, the oxygen of an amide carbonyl group of a second ligand is located at a short distance and acts as a fifth donor in these complexes. In the crystal obtained for **9b**, the Zn atom displays a clear square-pyramidal geometry coordinated to the four nitrogen atoms of a ligand and to the carbonyl oxygen of a second ligand. As observed in other C_2-symmetric pseudopeptidic ligands, the nature of the side chain of the component amino acid plays an important role in the fine-tuning of the properties of the corresponding complexes, affecting both the stability constants and the structural arrangement presented. Thus, for instance, the presence of the aromatic side chains in ligand **6** makes more difficult the coordination of the carbonyl group of the second ligand to the metal center in complexes **10a** and **10c**.

Finally, preliminary experiments reveal the capacity of some of the former complexes to act as catalysts for the ring-opening of the cyclohexene epoxide using aniline as the nucleophile in water. Interestingly, the results show that this is a ligand accelerated catalytic process and Zn^{2+} complexes act as more efficient catalysts, in particular, **10b** formed in the presence of ligand **6**, than the related Cu^{2+} complexes. Unfortunately, the catalytic reaction took place without any observed enantiomeric induction, although the studied Zn^{2+} complexes seem to present a higher catalytic activity than other systems studied for this reaction.

EXPERIMENTAL SECTION

All reagents and solvents were obtained from commercial sources and used as received unless otherwise stated. Deionized water was used from a "Milli-Q Integral Water Purification System" by Millipore. Microanalyses were performed on an elemental analyzer equipped with an oxygen module. Rotatory power was determined with a digital polarimeter (Na: 589 nm). Melting points were measured using a standard apparatus and are uncorrected.

^{1}H NMR Experiments. ^{1}H spectra were recorded on a Varian INOVA 500 spectrometer (500 and 125 MHz for ^{1}H and ^{13}C NMR, respectively). The solvent signal was used as a reference standard.

Electromotive Force Measurements and UV−vis Experiments. The potentiometric titrations were carried out at 298 K using 0.1 M NaCl or 0.1 M NaCl/CH_3CN 7/3 v/v as the supporting electrolyte. The experimental procedure (buret, potentiometer, cell, stirrer, microcomputer, etc.) has been fully described elsewhere.[41] The acquisition of the emf data was performed with the computer program CrisonCapture. The reference electrode was a Ag/AgCl electrode in saturated KCl solution. The glass electrode was calibrated as a hydrogen-ion concentration probe by titration of previously standardized amounts of HCl with CO_2-free NaOH solutions, and the equivalence point was determined by the Gran's method,[42] which gives the standard potential, $E°'$, and the ionic product of water 13.78, whereas, in the case of the water/ACN mixture used, this value was 14.6.[27] The computer program HYPERQUAD[26] was used to calculate the protonation and stability constants, and the HySS[43] program was used to obtain the distribution diagrams. The pH range investigated was 2.0−12.0, and the concentration of the metal ions and of the ligands 0.1 mM with M^{2+}:L molar ratios as 1:1. The different titration curves for each system (at least two) were treated either as a single set or as separated curves without significant variations in the values of the stability constants. Finally, the sets of data were merged together and treated simultaneously to give the final stability constants.

UV−vis absorption spectra were recorded using a Hewlett-Packard 8453 device, using solutions of 0.1 mM at different pH values

DOI: 10.1021/acs.inorgchem.6b01066
Inorg. Chem. XXXX, XXX, XXX−XXX

containing 1:1 M^{2+}:L molar ratios. Additional experiments were carried out in 0.1 M NaCl solutions. Only minimal differences were observed in this case.

Mass Spectrometry. Mass spectra were recorded on a Q-TOF Premier mass spectrometer with an orthogonal Z-spray electrospray interface (Micromass, Manchester, U.K.) either by electrospray positive mode (ES^+) or by electrospray negative mode (ES^-). The desolvation gas, as well as nebulizing gas, was nitrogen at a flow of 700 and 20 L/h, respectively. The temperature of the source block was set to 120 °C and the desolvation temperature to 150 °C. A capillary voltage of 3.5 and 3.3 kV was used in the positive and negative scan mode, respectively. The cone voltage was typically set to 20 V to control the extent of fragmentation of the identified ions. Sample solutions were infused via syringe pump directly connected to the ESI source at a flow rate of 10 mL/min. The observed isotopic pattern of each intermediate perfectly matched the theoretical isotope pattern calculated from their elemental composition using the MassLynx 4.0 program.[44]

IR Spectroscopy. FT-IR spectra were acquired on a JASCO 6200 equipment with a MIRacle single reflection ATR diamond/ZnSe accessory. The raw IR spectral data were processed with the JASCO spectral manager software.

Crystallography. Single crystals of ligand **6** and complexes **9a**−**c** and **10a**, **10c** were obtained. A suitable crystal was selected and measured on a single crystal X-ray diffractometer. Using Olex2,[45] all the structures were solved with the ShelXS 2014[46] structure solution program using Direct Methods and refined with the ShelXL 2014[46] refinement package using Least Squares minimization. The programs MERCURY[47] and PyMOL[48] were used to prepare artwork representations. Crystallographic data and refinement parameters are summarized in Table 4 and Tables S1 and S2. Hydrogen bonds for the compounds are grouped in Tables S3−S7. Crystallographic details are available in the Supporting Information in CIF format: CCDC numbers 1474242 (**9b**), 1474243 (**10a**), 1474244 (**6**), 1474245 (**10c**), 1474246 (**9c**), 1474247 (**9a**).

Synthesis of Compounds. *Compound* ***3***. Cbz-Val-OH (10.0 g, 39.0 mmol) and triethyl amine (5.48 mL, 39.0 mmol) were dissolved, under a nitrogen atmosphere, in dry THF (200 mL). The reaction mixture was cooled with an ice bath and NaCl to −10 °C. Previously cooled ethyl chloroformate (3.84 mL, 39.0 mmol) was then added dropwise, and the reaction mixture was stirred for 30 min at −10 °C. Afterward, 1,2-phenylenediamine (2.13 g, 19.5 mmol) dissolved in 25 mL of dry THF was added dropwise, avoiding any increase of the temperature. After stirring for an additional 2 h at this temperature, it was left to warm up to room temperature, the stirring being continued for 24 h. The white precipitate formed was filtered, washed with water, and vacuum-dried. Yield 57% (6.53 g, 11.4 mmol); mp 206−208 °C; $[\alpha]_D^{25}$ + 3.08 (c = 0.01, DMSO); IR (ATR) 3289, 2961, 1690, 1652, 1594, 1533, 1497, 1454 cm^{-1}; ^1H NMR (500 MHz, DMSO-d_6) δ 9.44 (s, 2H), 7.52 (s, 2H), 7.46 (d, J = 7.5 Hz, 2H), 7.38−7.27 (m, 10H), 7.18 (dd, J = 5.9, 3.5 Hz, 2H), 5.11−5.01 (m, 4H), 4.01 (t, J = 7.2 Hz, 2H), 2.09 (d, J = 6.4 Hz, 2H), 0.91 (t, J = 6.0 Hz, 12H); ^{13}C NMR (75 MHz, DMSO-d_6) δ 170.9, 156.7, 137.2, 130.5, 128.8, 127.9, 125.2, 65.9, 61.5, 30.5, 19.4, 18.6; Anal. Calcd (%) for $C_{32}H_{38}N_4O_6$: C, 66.9; H, 6.7; N, 9.8. Found: C, 66.3; H, 6.5; N, 9.8.

Compound ***5***. To a solution of compound **3** (1.20 g, 2.09 mmol) in dry MeOH in a two-neck round-bottom flask was added 10 mol % of the catalyst (5 wt % Pd on activated carbon). The system was purged to remove the air and connected to a H_2 atmosphere (H_2 balloon) and stirred at room temperature for 8 h. The gray suspension turned black, and the precipitate was filtered off through a Celite bed and washed with MeOH. Evaporation of the solvent under vacuum yielded compound **5** as a white solid. Yield 66% (0.420 g, 1.37 mmol); mp 70−72 °C; $[\alpha]_D^{25}$ − 15.34 (c = 0.01, $CHCl_3$); IR (ATR) 3298, 2959, 2930, 2872, 1661, 1599, 1506, 1465 cm^{-1}; ^1H NMR (500 MHz, $CDCl_3$) δ 9.55 (s, 2H), 7.61 (dd, J = 5.9, 3.6 Hz, 2H), 7.19 (dd, J = 6.0, 3.5 Hz, 2H), 3.39 (s, 2H), 2.44−2.33 (m, 2H), 1.07 (d, J = 7.0 Hz, 6H), 0.93 (d, J = 6.9 Hz, 6H); ^{13}C NMR (75 MHz, $CDCl_3$) δ 173.5, 130.0, 126.0, 124.5, 61.0, 31.4, 19.7, 16.3; HRMS (ESI-TOF)$^+$ Calcd for $C_{16}H_{26}N_4O_2$ (M + H^+) 307.2134. Found 307.2131; Anal. Calcd (%) for $C_{16}H_{26}N_4O_2$·0.5 H_2O: C, 60.9; H, 8.6 N, 17.8. Found: C, 61.5; H, 8.1; N, 17.4.

Compound ***4***. Prepared using the same protocol described for **3** but starting from Cbz-Phe-OH. Yield 39% (4.39 g, 6.55 mmol); mp 201−203 °C; $[\alpha]_D^{25}$ + 4.84 (c = 0.01, DMSO); IR (ATR) 3302, 3256, 3062, 2918, 1652, 1527, 1255 cm^{-1}; ^1H NMR (500 MHz, DMSO-d_6) δ 9.55 (s, 2H), 7.65 (d, J = 7.4 Hz, 1H), 7.49 (s, 1H), 7.32−7.02 (m, 10H), 4.93 (dd, J = 51.5, 12.6 Hz, 4H), 4.44 (s, 2H), 3.01−2.84 (m, 2H); ^{13}C NMR (75 MHz, DMSO-d_6) δ 171.1, 138.3, 137.3, 130.8, 129.7, 128.7, 128.5, 128.1, 127.9, 126.8, 125.8, 125.3, 65.9, 57.3, 37.6; Anal. Calcd (%) for $C_{40}H_{38}N_4O_6$·0.5 H_2O: C, 70.7; H, 5.8; N, 8.2. Found: C, 70.4; H, 5.6; N, 7.9.

Compound ***6***. Prepared using the same protocol described for **5** but starting from **4**. Yield 53% (0.33 g, 0.81 mmol); mp 110−113 °C; $[\alpha]_D^{25}$ + 111.13 (c = 0.01, $CHCl_3$); IR (ATR) 3373, 3298, 3026, 2918, 1671, 1509, 1452 cm^{-1}; ^1H NMR (500 MHz, $CDCl_3$) δ 9.47 (s, 1H), 7.61 (dd, J = 5.9, 3.6 Hz, 2H), 7.32 (dd, J = 20.0, 12.5 Hz, 4H), 7.27−7.20 (m, 6H), 3.76 (dd, J = 9.2, 4.1 Hz, 2H), 3.34 (dd, J = 13.7, 4.0 Hz, 2H), 2.80 (dd, J = 13.7, 9.2 Hz, 2H); ^{13}C NMR (75 MHz, $CDCl_3$) δ 172.8, 137.4, 129.8, 129.3, 128.8, 126.8, 126.0, 124.5, 56.9, 40.9; HRMS (ESI-TOF)$^+$ Calcd for $C_{24}H_{26}N_4O_2$ (M + H^+) 403.2134. Found 403.2139; Anal. Calcd (%) for $C_{24}H_{26}N_4O_2$·0.2 H_2O: C, 71.0; H, 6.6; N, 13.8. Found: C, 70.9; H, 6.3; N, 13.5.

General Procedure for the Synthesis of Cu^{2+} Complexes. *Complex* ***9a***. A solution of $Cu(OAc)_2$ (1 equiv) in MeOH (*ca.* 10^{-2} M) was added to a solution of compound **5** (1 equiv) in MeOH (*ca.* 10^{-2} M). After stirring the mixture for 30 min at room temperature, KOH (*ca.* 2 equiv) 1 M in methanol was added, and the solution was maintained at room temperature overnight. The precipitate formed was isolated by filtration and washed with dichloromethane, to yield a purple powder. Yield 73% (0.10 g, 0.28 mmol); (IR) ATR 3600−3000, 2963, 2960, 1591, 1537, 1469, 1395 cm^{-1}; Anal. Calcd (%) for $C_{16}H_{24}N_4O_2Cu$·H_2O: C, 49.8; H, 6.8; N, 14.5. Found: C, 49.3; H, 6.8; N, 14.4.

Complex ***10a***. Yield 84% (0.076 g, 0.16 mmol); (IR) ATR 3600−3000, 2963, 1594, 1541, 1471 cm^{-1}; Anal. Calcd (%) for $C_{24}H_{24}N_4O_2Cu$: C, 62.1; H, 5.2; N, 12.1. Found: C, 62.1, H, 5.3, N, 12.0.

General Procedure for the Synthesis of Zn^{2+} Complexes. *Complex* ***9b***. A solution of $Zn(OAc)_2$ (1 equiv) in MeOH (*ca.* 10^{-2} M) was added to a solution of compound **5** (1 equiv) in MeOH (*ca.* 10^{-2} M). After stirring the mixture for 30 min at room temperature, KOH (*ca.* 2 equiv) 1 M in methanol was added, and the solution was maintained at room temperature overnight. The precipitate formed was isolated by filtration and washed with dichloromethane to yield a white solid. Yield 54% (0.434 g, 1.17 mmol); (IR) ATR 3600−3000, 1591, 1523, 1473 cm^{-1}; Anal. Calcd (%) for $C_{16}H_{24}N_4O_2Zn$·3 H_2O: C, 45.3; H, 7.1; N, 13.2. Found C, 45.6; H, 6.8; N, 13.1.

Complex ***10b***. Yield 41% (0.14 g, 0.31 mmol); (IR) ATR 3352−3308, 3248, 3144, 2963, 2960, 1591, 1537, 1469, 1395 cm^{-1}; Anal. Calcd (%) for $C_{24}H_{24}N_4O_2Zn$·0.1 H_2O: C, 61.6; H, 5.2; N, 12.0. Found C, 61.3, H, 5.3; N, 11.8.

General Procedure for the Synthesis of Ni^{2+} Complexes. *Complex* ***9c***. To a solution of $Ni(OAc)_2$ (1 equiv) in MeOH (*ca.* 10^{-2} M) was added to a solution of compound **5** (1 equiv) in MeOH (*ca.* 10^{-2} M). After stirring the mixture for 30 min at room temperature, KOH (*ca.* 2 equiv) 1 M in methanol was added, and the solution was maintained at room temperature overnight. The precipitate formed was isolated by filtration and washed with dichloromethane to yield a yellow solid. Yield 67% (0.091 g, 0.25 mmol); (IR) ATR 3396−3274, 2961, 1594, 1551, 1494 cm^{-1}; Anal. Calcd (%) for $C_{16}H_{24}N_4O_2Ni$·C_2H_5OH: C, 52.8; H, 7.4; N, 13.7. Found: C, 52.8; H, 7.3; N, 13.7.

Complex ***10c***. Yield 78% (0.067 g, 0.14 mmol); (IR) ATR 3281−3026, 2940, 2918, 1597, 1551, 1476, 1452, 1275 cm^{-1}; Anal. Calcd (%) for $C_{24}H_{24}N_4O_2Ni$·H_2O: C, 60.4; H, 5.5; N, 11.7. Found: C, 60.6, H, 5.3, N, 11.7.

Typical Procedure for Ring-Opening of Epoxide Reaction. In an oven-dried 5 mL vial, the bis(amino amide) (0.05 mmol) and the metal acetate (0.05 mmol) were dissolved in 2 mL of solvent, and the vial was closed. After 30 min stirring, cyclohexene oxide (103 μL, 1.0 mmol) was added. After 1 h stirring at room temperature, aniline (92

DOI: 10.1021/acs.inorgchem.6b01066
Inorg. Chem. XXXX, XXX, XXX−XXX

μL, 1.0 mmol) was added, and the mixture stirred for 16 h. The solvent was evaporated to dryness, and the residue was dissolved in water (5 mL) and extracted with DCM (3 × 5 mL). The organic phases were collected and dried over anhydrous $MgSO_4$ and evaporated to give pure 2-phenyl amino cyclohexanol. ^{1}H NMR (500 MHz, $CDCl_3$) δ 7.22−7.11 (m, 2H), 6.80−6.63 (m, 3H), 3.38−3.32 (m, 1H), 3.15 (ddd, *J* = 11.2, 9.2, 4.0 Hz, 1H), 2.20−2.03 (m, 2H), 1.83−1.63 (m, 2H), 1.47−1.21 (m, 3H), 1.06 (ddd, *J* = 24.1, 12.8, 3.7 Hz, 1H).

■ ASSOCIATED CONTENT

Supporting Information

The Supporting Information is available free of charge on the ACS Publications website at DOI: 10.1021/acs.inorgchem.6b01066.

Characterization of the compounds **5** and **6**, ^{1}H NMR titration of compound **5** at different pH values, potentiometric distribution diagrams, FT-IR spectroscopy, ESI-MS spectra, X-ray crystallographic data (PDF)
Crystallographic data for **6**, **9a**, **9b**, **9c**, **10a**, and **10c** (CIF)

■ AUTHOR INFORMATION

Corresponding Authors

*E-mail: luiss@uji.es (S.V.L.).
*E-mail: altava@uji.es (B.A.).

Notes

The authors declare no competing financial interest.

■ ACKNOWLEDGMENTS

This research work was supported by the Spanish MINECO (CTQ2015-68429-R), Generalitat Valenciana (PROMETEO/2012/020), and PPI-UJI (P1-1B-2013-38). L.G. thanks Generalitat Valenciana for a Santiago Grisolia fellowship (GRISOLIA 2012/015). The support of the SCIC for the different instrumental techniques at Universitat Jaume I is acknowledged.

■ REFERENCES

(1) (a) Multhaup, G.; Schlicksupp, A.; Hesse, L.; Beher, D.; Ruppert, T.; Masters, C. L.; Beyreuther, K. *Science* **1996**, *271*, 1406−1409. (b) Sen, C. K.; Khanna, S.; Venojarvi, M.; Trikha, P.; Ellison, E. C.; Hunt, T. K.; Roy, S. *Am. J. Physiol. Heart Circ. Physiol.* **2002**, *282*, H1821−H1827. (c) Grubman, A.; White, A. R. *Expert Rev. Mol. Med.* **2014**, *16*, e11. (d) Scheiber, I. F.; Mercer, J. F. B.; Dringen, R. *Prog. Neurobiol.* **2014**, *116*, 33−57. (e) Bellingham, S. A.; Guo, B.; Hill, A. F. *Biol. Cell* **2015**, *107*, 389−418.

(2) (a) Fricker, S. P. *Dalton Trans.* **2007**, 4903−4917. (b) Mjos, K. D.; Orvig, C. *Chem. Rev.* **2014**, *114*, 4540−4563. (c) Medici, S.; Peana, M.; Nurchi, V. M.; Lachowicz, J. I.; Crisponi, G.; Zoroddu, M. A. *Coord. Chem. Rev.* **2015**, *284*, 329−350.

(3) (a) Crichton, R. R.; Dexter, D. T.; Ward, R. J. *Coord. Chem. Rev.* **2008**, *252*, 1189−1199. (b) Ward, R. J.; Dexter, D. T.; Crichton, R. R. *Curr. Med. Chem.* **2012**, *19*, 2760−2772.

(4) (a) Cini, R.; Tamasi, G.; Defazio, S.; Hursthouse, M. B. *J. Inorg. Biochem.* **2007**, *101*, 1140−1152. (b) Marzano, C.; Pellei, M.; Tisato, F.; Santini, C. *Anti-Cancer Agents Med. Chem.* **2009**, *9*, 185−211.

(5) (a) Sousa, I.; Claro, V.; Pereira, J. L.; Amaral, A. L.; Cunha-Silva, L.; de Castro, B.; Feio, M. J.; Pereira, E.; Gameiro, P. *J. Inorg. Biochem.* **2012**, *110*, 64−71. (b) Dorotikova, S.; Koziskova, J.; Malcek, M.; Jomova, K.; Herich, P.; Plevova, K.; Briestenska, K.; Chalupkova, A.; Mistrikova, J.; Milata, V.; Dvoranova, D.; Bucinsky, L. *J. Inorg. Biochem.* **2015**, *150*, 160−173.

(6) Sönmez, M.; Levent, A.; Şekerci, M. *Russ. J. Coord. Chem.* **2004**, *30*, 655−660.

(7) (a) Miyake, H.; Kojima, Y. *Coord. Chem. Rev.* **1996**, *148*, 301−314. (b) Wende, C.; Lüdtke, C.; Kulak, N. *Eur. J. Inorg. Chem.* **2014**, *2014*, 2597−2612. (c) Quintanova, C.; Keri, R. S.; Chaves, S.; Santos, M. A. *J. Inorg. Biochem.* **2015**, *151*, 58−66. (d) Skalamera, D.; Sanders, E.; Vianello, R.; Marsavelski, A.; Pevec, A.; Turel, I.; Kirin, S. I. *Dalton Trans.* **2016**, *45*, 2845−2858.

(8) (a) Karlin, K. *Science* **1993**, *261*, 701−708. (b) Roat-Malone, R. M. *Bioinorganic Chemistry: A Short Course*, 2nd ed.; John Wiley & Sons, Inc.: Hoboken, NJ, 2007. (c) Gray, H. B.; Stiefel, E. I.; Valentine, J. S.; Bertini, I. *Biological Inorganic Chemistry: Structure and Reactivity*, 1st ed.; University Science Books: Sausalito, CA, 2007. (d) Gramage-Doria, R.; Armspach, D.; Matt, D. *Coord. Chem. Rev.* **2013**, *257*, 776−816. (e) Bistri, O.; Reinaud, O. *Org. Biomol. Chem.* **2015**, *13*, 2849−2865.

(9) (a) Hechavarría Fonseca, M.; König, B. *Adv. Synth. Catal.* **2003**, *345*, 1173−1185. (b) Green, B. J.; Tesfai, T. M.; Xie, Y.; Margerum, D. W. *Inorg. Chem.* **2004**, *43*, 1463−1471. (c) Tesfai, T. M.; Green, B. J.; Margerum, D. W. *Inorg. Chem.* **2004**, *43*, 6726−6733. (d) Prell, J. S.; Flick, T. G.; Oomens, J.; Berden, G.; Williams, E. R. *J. Phys. Chem. A* **2010**, *114*, 854−860. (e) Dokorou, V. N.; Milios, C. J.; Tsipis, A. C.; Haukka, M.; Weidler, P. G.; Powell, A. K.; Kostakis, G. E. *Dalton Trans.* **2012**, *41*, 12501−12513. (f) Dennis, C. R.; Swarts, J. C.; Margerum, D. W. *React. Kinet., Mech. Catal.* **2012**, *107*, 27−38. (g) Dong, J.; Wang, Y.; Xiang, Q.; Lv, X.; Weng, W.; Zeng, Q. *Adv. Synth. Catal.* **2013**, *355*, 692−696.

(10) (a) Locardi, E.; Stöckle, M.; Gruner, S.; Kessler, H. *J. Am. Chem. Soc.* **2001**, *123*, 8189−8196. (b) Gibson, S. E.; Lecci, C. *Angew. Chem., Int. Ed.* **2006**, *45*, 1364−1377. (c) White, C. J.; Yudin, A. K. *Nat. Chem.* **2011**, *3*, 509−524. (d) Lewandowski, B.; De Bo, G.; Ward, J. W.; Papmeyer, M.; Kuschel, S.; Aldegunde, M. J.; Gramlich, P. M. E.; Heckmann, D.; Goldup, S. M.; D'Souza, D. M.; Fernandes, A. E.; Leigh, D. A. *Science* **2013**, *339*, 189−193.

(11) (a) Fernandez-Lopez, S.; Kim, H.-S.; Choi, E. C.; Delgado, M.; Granja, J. R.; Khasanov, A.; Kraehenbuehl, K.; Long, G.; Weinberger, D. A.; Wilcoxen, K. M.; Ghadiri, M. R. *Nature* **2001**, *412*, 452−455. (b) Kubik, S. *Chem. Soc. Rev.* **2009**, *38*, 585−605. (c) Klemm, K.; Radić Stojković, M.; Horvat, G.; Tomišić, V.; Piantanida, I.; Schmuck, C. *Chem.—Eur. J.* **2012**, *18*, 1352−1363.

(12) (a) Hu, X.; Nguyen, K. T.; Verlinde, C. L. M. J.; Hol, W. G. J.; Pei, D. *J. Med. Chem.* **2003**, *46*, 3771−3774. (b) Loughlin, W. A.; Tyndall, J. D. A.; Glenn, M. P.; Fairlie, D. P. *Chem. Rev.* **2004**, *104*, 6085−6118. (c) Silva, G. A.; Czeisler, C.; Niece, K. L.; Beniash, E.; Harrington, D. A.; Kessler, J. A.; Stupp, S. I. *Science* **2004**, *303*, 1352−1355.

(13) (a) Choi, K.; Hamilton, A. D. *Coord. Chem. Rev.* **2003**, *240*, 101−110. (b) Wu, Y.-D.; Gellman, S. *Acc. Chem. Res.* **2008**, *41*, 1231−1232. (c) Nowick, J. S. *Acc. Chem. Res.* **2008**, *41*, 1319−1330. (d) Suzuki, M.; Hanabusa, K. *Chem. Soc. Rev.* **2009**, *38*, 967−975. (e) Brea, R. J.; Reiriz, C.; Granja, J. R. *Chem. Soc. Rev.* **2010**, *39*, 1448−1456. (f) Ke, D.; Zhan, C.; Li, A. D. Q.; Yao, J. *Angew. Chem., Int. Ed.* **2011**, *50*, 3715−3719. (g) Das, D.; Maiti, S.; Brahmachari, S.; Das, P. K. *Soft Matter* **2011**, *7*, 7291−7303.

(14) (a) Merschky, M.; Schmuck, C. *Org. Biomol. Chem.* **2009**, *7*, 4895−4903. (b) Weseliński, Ł.; Słyk, E.; Jurczak, J. *Tetrahedron Lett.* **2011**, *52*, 381−384. (c) Paradowska, J.; Pasternak, M.; Gut, B.; Gryzło, B.; Mlynarski, J. *J. Org. Chem.* **2012**, *77*, 173−187.

(15) (a) Dangel, B.; Clarke, M.; Haley, J.; Sames, D.; Polt, R. *J. Am. Chem. Soc.* **1997**, *119*, 10865−10866. (b) Dangel, B. D.; Polt, R. *Org. Lett.* **2000**, *2*, 3003−3006. (c) Polt, R.; Kelly, B. D.; Dangel, B. D.; Tadikonda, U. B.; Ross, R. E.; Raitsimring, A. M.; Astashkin, A. V. *Inorg. Chem.* **2003**, *42*, 566−574.

(16) (a) Luis, S. V.; Alfonso, I. *Acc. Chem. Res.* **2014**, *47*, 112−124.

(17) (a) Galindo, F.; Becerril, J.; Isabel Burguete, M.; Luis, S. V.; Vigara, L. *Tetrahedron Lett.* **2004**, *45*, 1659−1662. (b) Alfonso, I.; Burguete, M. I.; Galindo, F.; Luis, S. V.; Vigara, L. *J. Org. Chem.* **2009**, *74*, 6130−6142. (c) Altava, B.; Burguete, M. I.; Carbó, N.; Escorihuela, J.; Luis, S. V. *Tetrahedron: Asymmetry* **2010**, *21*, 982−989. (d) Martí-Centelles, V.; Izquierdo, M. A.; Burguete, M. I.; Galindo, F.; Luis, S. V. *Chem.—Eur. J.* **2014**, *20*, 7465−7478. (e) Faggi, E.; Moure, A.; Bolte,

DOI: 10.1021/acs.inorgchem.6b01066
Inorg. Chem. XXXX, XXX, XXX−XXX

M.; Vicent, C.; Luis, S. V.; Alfonso, I. *J. Org. Chem.* **2014**, *79*, 4590−4601.
(18) (a) Alfonso, I.; Burguete, M. I.; Luis, S. V. *J. Org. Chem.* **2006**, *71*, 2242−2250. (b) Alfonso, I.; Burguete, M. I.; Galindo, F.; Luis, S. V.; Vigara, L. *J. Org. Chem.* **2007**, *72*, 7947−7956. (c) Faggi, E.; Luis, S. V.; Alfonso, I. *RSC Adv.* **2013**, *3*, 11556−11565.
(19) (a) Becerril, J.; Burguete, M. I.; Escuder, B.; Galindo, F.; Gavara, R.; Miravet, J. F.; Luis, S. V.; Peris, G. *Chem.—Eur. J.* **2004**, *10*, 3879−3890. (b) Becerril, J.; Escuder, B.; Miravet, J. F.; Gavara, R.; Luis, S. V. *Eur. J. Org. Chem.* **2005**, *2005*, 481−485. (c) Wadhavane, P. D.; Galian, R. E.; Izquierdo, M. A.; Aguilera-Sigalat, J.; Galindo, F.; Schmidt, L.; Burguete, M. I.; Perez-Prieto, J.; Luis, S. V. *J. Am. Chem. Soc.* **2012**, *134*, 20554−20563. (d) Rubio, J.; Martí-Centelles, V.; Burguete, M. I.; Luis, S. V. *Tetrahedron* **2013**, *69*, 2302−2308.
(20) (a) Galindo, F.; Burguete, M. I.; Vigara, L.; Luis, S. V.; Kabir, N.; Gavrilovic, J.; Russell, D. A. *Angew. Chem., Int. Ed.* **2005**, *44*, 6504−6508. (b) Wadhavane, P. D.; Izquierdo, M. A.; Lutters, D.; Burguete, M. I.; Marin, M. J.; Russell, D. A.; Galindo, F.; Luis, S. V. *Org. Biomol. Chem.* **2014**, *12*, 823−831.
(21) Adrián, F.; Burguete, M. I.; Fraile, J. M.; García, J. I.; García, J.; García-España, E.; Luis, S. V.; Mayoral, J. A.; Royo, A. J.; Sánchez, M. C. *Eur. J. Inorg. Chem.* **1999**, *1999*, 2347−2354.
(22) (a) Blasco, S.; Burguete, M. I.; Clares, M. P.; García-España, E.; Escorihuela, J.; Luis, S. V. *Inorg. Chem.* **2010**, *49*, 7841−7852. (b) Martí, I.; Ferrer, A.; Escorihuela, J.; Burguete, M. I.; Luis, S. V. *Dalton Trans.* **2012**, *41*, 6764−6776. (c) Wadhavane, P. D.; Gorla, L.; Ferrer, A.; Altava, B.; Burguete, M. I.; Izquierdo, M. A.; Luis, S. V. *RSC Adv.* **2015**, *5*, 72579−72589.
(23) Marti-Centelles, V.; Kumar, D. K.; White, A. J. P.; Luis, S. V.; Vilar, R. *CrystEngComm* **2011**, *13*, 6997−7008.
(24) Martell, A. E.; Motekaitis, R. J. *Coord. Chem. Rev.* **1990**, *100*, 323−361.
(25) García-España, E.; Díaz, P.; Llinares, J. M.; Bianchi, A. *Coord. Chem. Rev.* **2006**, *250*, 2952−2986.
(26) Gans, P.; Sabatini, A.; Vacca, A. *Talanta* **1996**, *43*, 1739−1753.
(27) Herrador, M. Á.; González, A. G. *Talanta* **2002**, *56*, 769−775.
(28) (a) Bianchi, A.; Escuder, B.; García-España, E.; Luis, S. V.; Marcelino, V.; Miravet, J. F.; Ramirez, J. A. *J. Chem. Soc., Perkin Trans. 2* **1994**, 1253−1259. (b) Aguilar, J. A.; García-España, E.; Guerrero, J.; Luis, S. V.; Llinares, J.; Ramírez, J.; Soriano, C. *Inorg. Chim. Acta* **1996**, *246*, 287−294. (c) Arán, V. J.; Kumar, M.; Molina, J.; Lamarque, L.; Navarro, P.; García-España, E.; Ramírez, J. A.; Luis, S. V.; Escuder, B. *J. Org. Chem.* **1999**, *64*, 6135−6146.
(29) (a) Pasquarello, A.; Petri, I.; Salmon, P. S.; Parisel, O.; Car, R.; Tóth, É.; Powell, D. H.; Fischer, H. E.; Helm, L.; Merbach, A. E. *Science* **2001**, *291*, 856−859. (b) Frank, P.; Benfatto, M.; Hedman, B.; Hodgson, K. O. *Inorg. Chem.* **2008**, *47*, 4126−4139. (c) Zitolo, A.; Chillemi, G.; D'Angelo, P. *Inorg. Chem.* **2012**, *51*, 8827−8833. (d) Constable, E. C.; Housecroft, C. E.; Price, J. R.; Zampese, J. A. *CrystEngComm* **2010**, *12*, 3163−3171. (e) Bukharov, M. S.; Shtyrlin, V. G.; Mamin, G. V.; Stapf, S.; Mattea, C.; Mukhtarov, A. S.; Serov, N. Y.; Gilyazetdinov, E. M. *Inorg. Chem.* **2015**, *54*, 9777−9784.
(30) (a) Autzen, S.; Korth, H.-G.; Boese, R.; de Groot, H.; Sustmann, R. *Eur. J. Inorg. Chem.* **2003**, *2003*, 1401−1410. (b) Pauly, M. A.; Erwin, E. M.; Powell, D. R.; Rowe, G. T.; Yang, L. *Polyhedron* **2015**, *102*, 722−734.
(31) (a) Schug, K.; Fryčák, P.; Maier, N. M.; Lindner, W. *Anal. Chem.* **2005**, *77*, 3660−3670. (b) Di Tullio, A.; Reale, S.; De Angelis, F. *J. Mass Spectrom.* **2005**, *40*, 845−865. (c) Baytekin, B.; Baytekin, H. T.; Schalley, C. A. *Org. Biomol. Chem.* **2006**, *4*, 2825−2841. (d) Beattie, J. W.; White, D. S.; Bheemaraju, A.; Martin, P. D.; Groysman, S. *Dalton Trans.* **2014**, *43*, 7979−7986.
(32) (a) Rebek, J. *Science* **1987**, *235*, 1478−1484. (b) Rebek, J. *Acc. Chem. Res.* **1990**, *23*, 399−404.
(33) (a) Dance, I. *New J. Chem.* **2003**, *27*, 22−27. (b) Álvarez, S. *Dalton Trans.* **2013**, *42*, 8617−8636. (c) White, N. G.; Serpell, C. J.; Beer, P. D. *Cryst. Growth Des.* **2014**, *14*, 3472−3479.
(34) (a) Alcón, M. J.; Iglesias, M.; Sánchez, F.; Viani, I. *J. Organomet. Chem.* **2000**, *601*, 284−292. (b) Burguete, M. I.; Collado, M.; Escorihuela, J.; Galindo, F.; García-Verdugo, E.; Luis, S. V.; Vicent, M. J. *Tetrahedron Lett.* **2003**, *44*, 6891−6894. (c) Xiong, Y.; Huang, X.; Gou, S.; Huang, J.; Wen, Y.; Feng, X. *Adv. Synth. Catal.* **2006**, *348*, 538−544. (d) Burguete, M. I.; Collado, M.; Escorihuela, J.; Luis, S. V. *Angew. Chem., Int. Ed.* **2007**, *46*, 9002−9005. (e) Xu, Z.; Daka, P.; Wang, H. *Chem. Commun.* **2009**, 6825−6827. (f) Albada, H. B.; Rosati, F.; Coquière, D.; Roelfes, G.; Liskamp, R. M. J. *Eur. J. Org. Chem.* **2011**, *2011*, 1714−1720.
(35) (a) Barbaro, P.; Bianchini, C.; Sernau, V. *Tetrahedron: Asymmetry* **1996**, *7*, 843−850. (b) Azizi, N.; Saidi, M. R. *Org. Lett.* **2005**, *7*, 3649−3651. (c) Bonollo, S.; Fringuelli, F.; Pizzo, F.; Vaccaro, L. *Green Chem.* **2006**, *8*, 960−964.
(36) (a) Sekar, G.; Singh, V. K. *J. Org. Chem.* **1999**, *64*, 287−289. (b) Yadav, J. S.; Reddy, A. R.; Narsaiah, A. V.; Reddy, B. V. S. *J. Mol. Catal. A: Chem.* **2007**, *261*, 207−212. (c) Shivani; Pujala, B.; Chakraborti, A. K. *J. Org. Chem.* **2007**, *72*, 3713−3722. (d) Bhanushali, M. J.; Nandurkar, N. S.; Bhor, M. D.; Bhanage, B. M. *Tetrahedron Lett.* **2008**, *49*, 3672−3676. (e) Li, Y.; Tan, Y.; Herdtweck, E.; Cokoja, M.; Kühn, F. E. *Appl. Catal., A* **2010**, *384*, 171−176. (f) Pujala, B.; Rana, S.; Chakraborti, A. K. *J. Org. Chem.* **2011**, *76*, 8768−8780. (g) Narsaiah, A. V.; Wadavrao, S. B.; Reddy, A. R.; Yadav, J. S. *Synthesis* **2011**, *2011*, 485−489. (h) Lu, H.-F.; Sun, L.-L.; Le, W.-J.; Yang, F.-F.; Zhou, J.-T.; Gao, Y.-H. *Tetrahedron Lett.* **2012**, *53*, 4267−4272. (i) Pathare, S. P.; Akamanchi, K. G. *Tetrahedron Lett.* **2013**, *54*, 6455−6459.
(37) (a) Schneider, C.; Sreekanth, A. R.; Mai, E. *Angew. Chem.* **2004**, *116*, 5809−5812. (b) Tschöp, A.; Marx, A.; Sreekanth, A. R.; Schneider, C. *Eur. J. Org. Chem.* **2007**, *2007*, 2318−2327.
(38) Bonollo, S.; Lanari, D.; Vaccaro, L. *Eur. J. Org. Chem.* **2011**, *2011*, 2587−2598.
(39) (a) Fan, R.-H.; Hou, X.-L. *J. Org. Chem.* **2003**, *68*, 726−730. (b) Wu, J.; Xia, H.-G. *Green Chem.* **2005**, *7*, 708−710.
(40) (a) Azoulay, S.; Manabe, K.; Kobayashi, S. *Org. Lett.* **2005**, *7*, 4593−4595. (b) Bonollo, S.; Fringuelli, F.; Pizzo, F.; Vaccaro, L. *Synlett* **2008**, *2008*, 1574−1578. (c) Kokubo, M.; Naito, T.; Kobayashi, S. *Tetrahedron* **2010**, *66*, 1111−1118.
(41) García- España, E.; Ballester, M.-J.; Lloret, F.; Moratal, J. M.; Faus, J.; Bianchi, A. *J. Chem. Soc., Dalton Trans.* **1988**, 101−104.
(42) (a) Gran, G. *Analyst* **1952**, *77*, 661−671. (b) Rossotti, F. J. C.; Rossotti, H. J. *J. Chem. Educ.* **1965**, *42*, 375−378.
(43) Alderighi, L.; Gans, P.; Ienco, A.; Peters, D.; Sabatini, A.; Vacca, A. *Coord. Chem. Rev.* **1999**, *184*, 311−318.
(44) (a) *MassLynx Software, version 4.0*; Waters/Micromass UK Limited: Milford, MA, 2002. (b) Moco, S.; Bino, R. J.; Vorst, O.; Verhoeven, H. A.; de Groot, J.; van Beek, T. A.; Vervoort, J.; de Vos, C. H. R. *Plant Physiol.* **2006**, *141*, 1205−1218.
(45) Dolomanov, O. V.; Bourhis, L. J.; Gildea, R. J.; Howard, J. A. K.; Puschmann, H. J. *J. Appl. Crystallogr.* **2009**, *42*, 339−341.
(46) Sheldrick, G. M. *Acta Crystallogr., Sect. A: Found. Crystallogr.* **2008**, *64*, 112−122.
(47) Macrae, C. F.; Bruno, I. J.; Chisholm, J. A.; Edgington, P. R.; McCabe, P.; Pidcock, E.; Rodriguez-Monge, L.; Taylor, R.; van de Streek, J.; Wood, P. A. *J. Appl. Crystallogr.* **2008**, *41*, 466−470.
(48) Delano, W. L. The PyMOL Molecular Graphics System; Schrödinger, LLC: Cambridge, MA. http://www.pymol.org.

DOI: 10.1021/acs.inorgchem.6b01066
Inorg. Chem. XXXX, XXX, XXX−XXX